

A crystal plasticity phenomenological model to capture the non-linear shear response of carbon fibre reinforced composites

Wei Tan^{1*}, Brian G. Falzon²

¹ School of Engineering and Materials Science, Queen Mary University London, London, UK

² Advanced Composites Research Group, School of Mechanical and Aerospace Engineering,
Queen's University Belfast, Belfast, UK

*Corresponding author: Wei Tan (wei.tan@qmul.ac.uk)

Abstract

A hardening response is often observed for shear-dominated large deformation of Carbon Fibre Reinforced Plastics (CFRP). This non-linear response is often modelled by fitting a strain hardening law against experimental stress-strain curves. Inspired by a crystal plasticity framework, we develop a phenomenological model to capture matrix shearing and fibre rotation of CFRP under finite strain. This phenomenological model is first verified by simple shear and transverse compression tests, followed by comprehensive validations against measured stress-strain responses of unidirectional (UD) and cross-ply composite laminates subjected to quasi-static loading. The analytical and finite element predictions of CFRP lamina under simple shear loading confirm that the initial yielding is governed by the shear yield strength of the matrix, while the hardening behaviour is dependent on the modulus and rotation of the carbon fibres. This model accurately predicts the non-linear behaviour of CFRP under off-axis loading without the need of an empirical curve-fitted strain hardening law.

Keywords: Polymer-matrix composites (PMCs); Plastic deformation; Crystal plasticity; Computational modelling

1. Introduction

Carbon Fibre Reinforced Plastic (CFRP) composites are finding increasing utilisation in 'lightweighting' applications due to their high specific stiffness and strength. The failure modes of these composites has been shown to be greatly affected by the material's shear characteristics [1]. Under transverse or shear loading, the main response of a unidirectional (UD) CFRP is controlled by the matrix, exhibiting large non-linear deformation and subsequent matrix cracking [2], see Figure 1. This non-linear hardening may be exploited in the design of fail-safe engineering structures. It is therefore essential to understand and be able to characterise the non-linear stress-strain responses of CFRP to determine design allowables for engineering composite structures. Non-linear behaviour may be observed in off-axis compression tests of unidirectional laminates [3], tensile or compressive loading on $\pm 45^\circ$ laminates [4–6] or V-notched rail shear test on cross-ply laminates [2,7]. A significant amount of fibre rotation can be observed in these samples [2,5]. It is therefore logical to consider the fibre rotation and matrix yielding in a constitutive model in order to accurately predict the material response under large deformations. Material models of composite laminates typically comprise a stress-strain constitutive model, a failure initiation criterion, and a damage evolution law that degrades the material modulus and sets the final failure state [8–10]. These models either assume a purely-elastic constitutive model or capture the non-linear behaviour by fitting mathematic curves to the experimental stress-strain hardening law [2,6,9,11–15]. In order to account for fibre rotation, 2D models based on infinitesimal strain assumption [4,5,16,17] use a geometrical relation between fibre rotation angle, φ ,

and local strains, ϵ_{xx} and ϵ_{yy} , by $\varphi = \tan^{-1}[(1 + \epsilon_{xx})/(1 + \epsilon_{yy})]$, which is only valid for symmetric $[\pm\theta]_{ns}$ composite laminates. Mandel et al. [18] and Laux [19] proposed non-associative plasticity models to describe yielding due to transverse and longitudinal shear loading, based on finite deformation theory. The fibre rotation was accounted for via a geometric equation. An elastic–viscoplastic constitutive model using invariant terms was proposed by Vogler and Koerber et al. [20,21] for capturing the non-linear behaviour. A yield function was defined, based on stress invariants, that remains unchanged for arbitrary coordinate system transformations with respect to the fibre direction. Therefore, the determination of yielding is independent of fibre rotation. developed based on the invariants of transverse isotropy for the non-linear behaviour of UD composite materials.

Dafalias [22] who introduced the concept of a ‘plastic spin’ effect within Hill’s plasticity model [23] developed a more general description of anisotropic non-linear plastic deformation. Dafalias modelled fibre rotation via a ‘plastic spin’ to describe the rotation of the material substructure (fibres) with respect to the overall material rotation. This involves the specification of additional tensorial constitutive rules for plastic spin based on the assumption that the material symmetries are invariant to plastic deformation. A similar strategy has recently been adopted by other researchers [24,25] to update the fibre rotation in the deformed configuration.

Rather than following the routes mentioned, a crystal plasticity model, originally developed for metals, is shown to also be capable of capturing the material anisotropy and the microstructure evolution [26–29] by analogy. It assumes that plastic flow through the crystal is due to shearing of the matrix and plastic slip does not alter the initial crystal orientation. Therefore, the ‘plastic spin’ effect is automatically taken into account within the crystal plasticity framework. This crystal

plasticity model is ideal to capture fibre rotation, especially when the material is under finite deformation.

The purpose of the present study is to develop a phenomenological model for composite laminates under finite deformation, and to predict the mechanical behaviour under large matrix shearing and associated fibre rotation. A computational framework based on crystal plasticity is presented for composite laminates. The mechanisms of non-linear hardening are revealed through analytical and finite element models. The fidelity of the phenomenological model is validated by comparing numerical results with measured stress-strain responses of UD and cross-ply composite laminates subjected to pure shear loading.

2. Phenomenological model

To develop a phenomenological constitutive model for CFRP composites, which can accurately model the fibre rotation and matrix shearing deformation, we shall proceed with a brief discussion of the deformation mechanisms of CFRP composite subjected to shear loading.

2.1 Experimental observations

The pure shear tests of unidirectional composite laminates conducted by Tan and Falzon [2] have shown that shear deformation is primarily the result of the shearing of the matrix along the fibre direction, without fibre rotation, when shear loading is applied parallel to the fibre direction. Based on these experimental observations, it is reasonable to postulate that plastic shear deformation of CFRP composites is mainly achieved by shearing of the matrix along certain ‘slip’ directions dictated by the fibres, as illustrated in Figure 1a. A direct consequence of this assumption is that under simple shear loading along the fibre direction, as shown in Figure 4a, there is

no fibre rotation. It should be noted that this is in contrast to the assumption used by other classical constitutive models (e.g., Hill's plasticity model [23]), where a non-zero fibre rotation, equal to half the engineering shear strain, $\gamma/2$, would be predicted.

Significant fibre rotation is observed when shear loading is applied perpendicular to the fibre orientation, Figure 1a. This effect is more evident when shear loading is applied to a cross-ply composite laminates as shown in Figure 1b [2,7]. The reorientation of fibres is confirmed by X-ray computer tomography, Figure 2. Therefore, our model needs to capture both matrix shearing deformation along the fibre direction, and fibre rotation.

2.2 Model assumptions

Experimental observations suggest that slip directions tend to follow the matrix-resin region or fibre-matrix interface [2,7,30,31]. The slip orientations can be categorised into two groups, longitudinal and transverse slip deformation, Figure 3. In the development of the phenomenological model, we adopt the classical framework of crystal plasticity [32,33], where the plastic deformation of a UD CFRP lamina is assumed, by analogy, to be due to fibre slip along certain slip systems within the matrix. We have defined six representative slip systems, as shown in Figure 4a and Table 1. For each slip system, α , we denote the slip direction vector, $s^{(\alpha)}$, and the slip plane normal vector, $m^{(\alpha)}$. For the local coordinate system (x_1, x_2, x_3) , x_1 aligns along the fibre direction and the (x_2, x_3) plane is perpendicular to the fibre direction. Note that slip along system $\alpha_L = 1,2,3$ represents the longitudinal slip of the lamina along the x_1 fibre direction, whilst $\alpha_T = 4,5,6$ represents the transverse slip of the lamina perpendicular to the x_1 fibre direction. Let β denote the minimum angle between the x_2 axis and the transverse slip system, α_T .

The typical longitudinal and transverse shears, along with their corresponding slip systems are illustrated in Figure 4b and Figure 4c. The notation of the slip systems is explained by the two following examples. For slip system $\alpha = 1$, the slip direction $(1, 0, 0)$ is aligned with the x_1 axis, while the slip plane normal $(0, 0, 1)$ is along the x_3 axis. Likewise, in the slip system $\alpha = 5$, the slip direction $(0, \cos \beta, \sin \beta)$ is in line with an inclined angle, β , with respect to the x_2 axis, while the slip plane normal $(0, -\sin \beta, \cos \beta)$ is the vector perpendicular to the slip direction. It is also noted that the longitudinal slip systems $\alpha_L = 2,3$ are also dependent on β .

The choice of transverse slip systems for CFRP lamina requires careful justification. The hexagonal closed packed (HCP) structure [34] within the (x_2, x_3) plane would result in α_T with $\beta = \pm 60^\circ$. When carbon fibres are not hexagonal closed packed, there are other potential slip directions depending on the yield criteria. Tresca's yield criterion [35] predicts transverse slip directions with angles $\beta = \pm 45^\circ$, where the material reaches its maximum shear stress. Puck's failure criterion [36], resembling the Mohr–Coulomb fracture hypothesis [37], suggests the transverse slip direction is around $\beta = \pm 37^\circ$. Note that in the Puck's model, the fracture plane angle, θ_{fp} , is defined as the angle between the fracture plane and x_3 axis, typically with $\theta_{fp} = \pm 53^\circ$. Puck's model introduces an additional fracture-resistance term due to internal friction. At the micro-mechanical level, the internal friction results from the normal stress acting on the micro-cracks in the matrix before failure [36]. Experimental results [30] as well as computational predictions [31,36,38,39] on the transverse compression failure of UD CFRP lamina also prove that the matrix is prone to fail along a certain plane of angle β in the range of $\beta = 37^\circ \pm 3^\circ$. Based on these physical considerations, we investigate the effect of transverse slip systems by selecting three groups of slip systems, α_T , as follows:

- (1) $\beta = 60^\circ$: Hexagonal closed packed structure.
- (2) $\beta = 45^\circ$: Tresca's yield criterion
- (3) $\beta = 37^\circ$: Puck's failure criterion and measured slip planes.

The effect of slip orientations on the mechanical response of UD CFRP subject to uniaxial transverse compression is discussed later in Section 4.2. It is emphasised that the precise orientation of slip systems depends on the microstructure (fibre distribution, fibre volume fraction, void contents, fibre/matrix interfacial properties [40] etc.) of composite lamina. For a general 3D load state, the orientation is not known *a priori* and is determined by the angle which maximises the failure criteria functions. Brent's algorithm, which combines a golden section search with parabolic interpolation, can be used for this purpose [11], considering that fibre slips will occur along either the matrix-rich area or the fibre-matrix interface.

2.3 Kinematics

Consider a UD CFRP lamina as shown in Figure 5 with fibre direction aligned along the x_1 coordinate. The total deformation gradient F_{ij} which maps the original configuration Ω_0 to Ω is multiplicatively decomposed into a plastic part F_{ij}^p which maps Ω_0 to an intermediate, stress free configuration Ω_i , and an elastic part F_{ij}^e which maps Ω_i to Ω , such that

$$F_{ij} = F_{ik}^e F_{kj}^p. \quad (1)$$

The plastic deformation of the lamina F_{kj}^p is characterized by the internal state variable, γ^α , representing the fibre slipping along an individual slip system, α . Let $s_i^{(\alpha)}$ and $m_i^{(\alpha)}$ denote the slip direction and slip normal vector respectively, F_{ij}^p may then be defined in rate form,

$$\dot{F}_{ij}^p = \sum_{\alpha=1}^N \dot{\gamma}^{(\alpha)} s_i^{(\alpha)} m_k^{(\alpha)} F_{kj}^p. \quad (2)$$

The orthogonal vectors $s_i^{(\alpha)}$ and $m_i^{(\alpha)}$ are assumed to rotate with the lamina, so in the deformed configuration, Ω , they become

$$s_i^{*(\alpha)} = F_{ij}^e s_j^{(\alpha)}, \quad (3)$$

$$m_i^{*(\alpha)} = m_j^{(\alpha)} (F_{ji}^e)^{-1}. \quad (4)$$

One of the goals of this paper is to understand the effect of fibre rotation on the stress-strain response, hence here we propose a way to evaluate the fibre rotation φ from the kinematic relation. Recall plastic spin does not change the fibre direction, therefore, φ can be evaluated from the elastic rotation R_{ij}^e of the lamina which is given by,

$$R_{ij}^e = F_{ik}^e (U_{jk}^e)^{-1}, \quad (5)$$

where R_{ij}^e is the rotation matrix, and U_{jk}^e is the right stretch tensor. Experimental observations [2] suggest that the fibre rotates about the x_3 axis, within the (x_1, x_2) plane. Therefore, the rotation matrix has the form below,

$$R_{ij}^e = \begin{bmatrix} \cos \varphi & -\sin \varphi & 0 \\ \sin \varphi & \cos \varphi & 0 \\ 0 & 0 & 1 \end{bmatrix}, \quad (6)$$

The fibre rotation φ is then calculated as,

$$\varphi = \tan^{-1}(R_{21}^e / R_{11}^e). \quad (7)$$

The elastic Green strain E_{ij}^e is given by

$$E_{ij}^e = \frac{1}{2} (F_{ki}^e F_{kj}^e - \delta_{ij}), \quad (8)$$

where δ_{ij} is the Kronecker delta.

2.4 Constitutive law

The UD lamina is assumed to be elastic and transversely isotropic. We define a material stress measurement, Σ_{ij} , in the intermediate configuration such that it is work conjugate to the elastic Green strain, E_{ij}^e . A linear elastic relationship is assumed between Σ_{ij} and E_{ij}^e with the elastic constitutive relationship given by,

$$\begin{pmatrix} E_{11}^e \\ E_{22}^e \\ E_{33}^e \\ E_{23}^e \\ E_{13}^e \\ E_{12}^e \end{pmatrix} = \begin{pmatrix} 1/E_f & -\nu_{21}/E_{m2} & -\nu_{31}/E_{m3} & 0 & 0 & 0 \\ -\nu_{12}/E_f & 1/E_{m2} & -\nu_{32}/E_{m3} & 0 & 0 & 0 \\ -\nu_{13}/E_f & -\nu_{23}/E_{m2} & 1/E_{m3} & 0 & 0 & 0 \\ 0 & 0 & 0 & 1/(2G_{23}) & 0 & 0 \\ 0 & 0 & 0 & 0 & 1/(2G_{13}) & 0 \\ 0 & 0 & 0 & 0 & 0 & 1/(2G_{12}) \end{pmatrix} \begin{pmatrix} \Sigma_{11} \\ \Sigma_{22} \\ \Sigma_{33} \\ \Sigma_{23} \\ \Sigma_{13} \\ \Sigma_{12} \end{pmatrix}, \quad (9)$$

where E_f is the longitudinal modulus of a UD lamina, E_{m2} and E_{m3} are the transverse moduli of the UD lamina in the x_2 and x_3 direction respectively. G_{ij} and ν_{ij} are the shear moduli and Poisson ratios respectively. Note that $G_{23} = 0.5E_m/(1 + \nu_{23})$ as a transversely isotropic material. The relationship between Cauchy stress, σ_{ij} , and material stress, Σ_{ij} , is given by:

$$\Sigma_{ij} = \det(F_{ij}^e) (F_{ik}^e)^{-1} \sigma_{kl} (F_{jl}^e)^{-1}. \quad (10)$$

It now remains to define the plastic constitutive relationship. Following Asaro and Needleman [32], the evolution of the shear strain, $\gamma^{(\alpha)}$, is given by a rate-dependent power law relationship,

$$\dot{\gamma}^{(\alpha)} = \dot{\gamma}_0 \left(\frac{\tau^{(\alpha)}}{\tau_y} \right)^n \text{sgn}[\tau^{(\alpha)}], \quad (11)$$

where $\tau^{(\alpha)}$ denotes the thermodynamic driving force for the shear strain rate $\dot{\gamma}^{(\alpha)}$, while τ_y and $\dot{\gamma}_0$ denotes the shear yield strength and the reference shear strain rate of the lamina respectively. n is a rate sensitivity exponent and $\text{sgn}[\]$ returns the sign of the resolved critical shear stress for determining the matrix yielding. In classical

crystal plasticity [33], the resolved shear stress $\tau^{(\alpha)}$ is evaluated from Schmid's law [41],

$$\tau^{(\alpha)} = s_i^{*(\alpha)} \sigma_{ij} m_j^{*(\alpha)}. \quad (12)$$

However, it has been shown that the yield strength of matrix material is pressure sensitive [42,43]. The pressure dependency is characterised by the friction coefficient, μ , and the transverse normal pressure, P , is introduced on the slip systems, similar to Mohr-Coulomb theory, such that the shear strength of a slip system, α , is given by,

$$\tau_y^{(\alpha)} = \begin{cases} \tau_y + \mu P & P \geq 0 \\ \tau_y & P < 0 \end{cases} \quad (13)$$

where τ_y is the shear yield strength in the absence of a pressure loading. As we assume the lamina is elastic along the fibre (x_1) direction, the pressure P is defined in the $x_2 - x_3$ plane and is given by:

$$P = -\frac{1}{2}(\Sigma_{22} + \Sigma_{33}). \quad (14)$$

3. Model implementation

3.1 Numerical implementation

The material model is implemented in ABAQUS Explicit (version 6.14) via the user subroutine VUMAT. The full algorithm is detailed in Appendix A of [44]. In brief, the subroutine collects the deformation gradient tensors and right stretch tensors, followed by the initialisation of slip systems for each integration point. Then intermediate stresses, Cauchy stresses, local shear strain rates and deformation gradient components are calculated for each slip system. During the calculation process, the analysis calculates the resolved shear stresses of each slip system.

Once any shear stress in the slip system reaches its critical resolved shear stress, the slip is activated and plastic flow is initiated. As the load is increased, the resolved shear stress on each system increases until the pressure-dependent shear yield strength, $\tau_y^{(\alpha)}$, is reached on one system. The fibre composite begins to plastically deform by slip on this system, termed the 'primary slip system'. As the load is increased further, $\tau_y^{(\alpha)}$ may be reached on other slip systems; these systems then begin to operate. Multiple slips may occur simultaneously during the loading process. Once the calculation loop finishes in each time increment, the subroutine will update the local plastic shear strain rate, deformation gradient and slip systems. The fibre rotation angle is stored as a state variable. The whole process is repeated for each element at every time increment.

3.2 Materials properties

IM7-8552 and AS4-PEKK carbon fibre unidirectional lamina are both modelled as an anisotropic, homogenised continuum with their slip systems defined in Section 2.2. The shear yielding of a lamina which is controlled by the matrix is defined by isotropic elastic, perfectly-plastic behaviour that satisfies the Von Mises yield criterion (J_2 flow theory). The longitudinal modulus, E_f , transverse modulus E_m , shear modulus G_{12} and shear yield strength τ_y of the lamina are measured from experiments. Material constants used for the finite element simulation are given in Table 2. The friction coefficient, μ , is chosen to be 0.28 according to [2]. The strain rate sensitivity, n , is calibrated against the measured yield strength at various strain rates [3,45]. Here, the strain rate sensitivity for IM7-8552 is $n = 22.4$. Although AS4-PEKK thermoplastic composites may have a higher strain rate sensitivity, we use the same parameter, n , in the absence of available experimental data. It should be

emphasised that in this study, all the virtual tests are within the quasi-static regime $\dot{\epsilon}=0.0004 \text{ s}^{-1}$. Therefore, the effect of the strain rate parameter, n , is negligible.

4. Finite element model

This section presents the predictive capabilities of the crystal plasticity model regarding the non-linear response of composite laminates. The geometrical hardening effect is explained by the analytical model of a simple shear test with a single element in Section 4.1. The effect of slip orientation, on the transverse compressive response of a single element, is shown in Section 4.2. Numerical results of off-axis compression tests of UD lamina, under various strain rates, is then compared against experimental results in Section 4.3. Finally, the capability of this micromechanical model, to capture the non-linear response of cross-ply composite laminates, is demonstrated in Section 4.4.

4.1 Simple shear tests of UD lamina

Simple shear loading parallel and perpendicular to the fibre orientation, see Figure 6a, were applied to a UD lamina (single element) under quasi-static deformation ($\dot{\gamma} = 10^{-4}/s$). The corresponding stress-strain curves are plotted in Figure 6b. Recall that the epoxy matrix is assumed to be perfectly plastic. For simple shear, parallel to the fibre direction, the curves predicted by the 'crystal model' capture the behaviour accurately. The matrix plastic deformation led to the localization of a shear band parallel to the fibres. The prediction from Hill's anisotropic yield criterion [23] under quasi-static loading rate is also shown in Figure 6b. Hill's model predicts an identical response for shear, parallel and perpendicular to the fibre directions, under quasi-static loading. It captures the initial yielding behaviour and matches the results predicted by the crystal plasticity model for small strain. However, for large shear

strain $\gamma > 8\%$, the stress-strain curve shows a downward trend, which is not physical compared to experiment. The two key assumptions of Hill's plasticity model [23] that lead to poor predictions of UD composite under simple shear loading are: (i) the material symmetries remain unchanged upon plastic deformation (ii) the kinematics of fibres are identical to the lamina. Hence the rotation of the local fibre coordinate system with respect to the global coordinate system is equal to the spin component of the total deformation gradient. In this simple shear case, Hill's model will rotate the local coordinates by $\gamma_{12}/2$ even though the fibre rotation is zero, hence leading to errors under finite deformation.

For simple shear, perpendicular to the fibre orientation, significant hardening behaviour is observed, which is consistent with shear experiments on UD lamina [2] and computational micromechanics prediction [31]. Assuming a perfect-bond between fibre and matrix, we derive the shear stress, τ_{12} , as a function of total shear strain γ , based on the crystal plasticity framework (see the detailed derivation in Appendix B of [44]),

$$\tau_{12} = \begin{cases} G_{12}\gamma & \gamma_p = 0 \\ \tau_y + 0.5E_f\gamma^3 & \gamma_p > 0 \end{cases}, \quad (15)$$

where $\gamma = \tan \omega$ is the total shear strain, γ_p the plastic strain and E_f the longitudinal modulus of composite lamina. The hardening behaviour is controlled by the term $0.5E_f\gamma^3$, which is the product of the longitudinal modulus of composite lamina E_f (dominated by the fibre modulus) and the cube of shear strain γ (indicating fibre rotation φ). The finite element prediction and analytical prediction are in a good agreement, confirming the accuracy of our crystal-plasticity based model. Physically, since matrix deformation could not progress independently of the fibres, significant fibre rotation is generated to accommodate the shear strain in the matrix and

inherently increases the Cauchy stress and corresponding resolved shear stress, Eq.(15). Consequently, a significant geometrical hardening response of the composite lamina under finite deformation is observed. However, due to fibre-matrix debonding, the measured stress-strain curves for shearing perpendicular to fibre direction [2] fail prematurely with a limited strain hardening behaviour observed. A significant strain hardening behaviour is evident in the cross-ply composite laminates due to the constraining effect of the adjacent plies

4.2 Transverse compression tests of UD lamina

As discussed earlier, Puck's model based on the Mohr–Coulomb hypothesis suggests that deformation of a composite lamina, under transverse compression, forms a fracture plane at an angle β to a plane parallel to the loading axis [30]. Similarly, in our crystal plasticity model, we define slip directions β . Applying uniaxial transverse compression to a composite lamina, the transverse compressive yield strength of the lamina, σ_y , is related to the critical resolved shear stress $\tau_y^{(\alpha)}$, see Appendix C of [44], note the in this paper, β is defined as the angle between slip plane and loading axis. The compressive yield strength of the lamina, σ_y , is given by,

$$\sigma_y = -\frac{2\tau_y^{(\alpha)}}{\sin 2\beta} . \quad (16)$$

To investigate the effect of slip orientation, β , upon the uniaxial compressive response of the composite lamina, virtual uniaxial compressive tests were conducted on a composite lamina with various slip systems, $\beta = 37^\circ$, 45° , and 60° . Their stress-strain responses are shown in Figure 6c. Note that for the case of a zero friction coefficient, $\mu = 0$, $\tau_y^{(\alpha)}$ equals the shear strength of the matrix $\tau_y = 62.3$ MPa. The compressive yield strength increases with increasing slip orientation from 45° to 60° . The predicted yield strength, with slip triggered at 45° , is close to the measured yield

strength, $\sigma_{my} = 104$ MPa [3]. In order to obtain accurate slip plane angles, Brent's algorithm that combines a golden section search with parabolic interpolation may be used [11], including the constraint that fracture planes mainly initiate and propagate along the fibre-matrix interface. For simplicity, the slip orientation in the transverse $y - z$ plane is set to be 45° for the following simulations. Figure 6c shows that compressive yield strengths, predicted by FE, are in a good agreement with the analytical solutions from Eq. (16), which confirm that matrix shearing deformation governs the transverse compression behaviour of a UD composite lamina.

4.3 Off-axis compression tests of UD composite lamina

In order to verify our model, we compare the finite element predictions with the measured stress-strain responses of a unidirectional (UD) composite subject to quasi-static off-axis compressive loading, as shown in Figure 7a.

Virtual off-axis compressive tests on composite laminates with fibre orientation angles $\theta=15^\circ$, 45° and 90° (transverse compression) were conducted. Quasi-static (QS) loading $\dot{\epsilon}_{QS} = 4 \times 10^{-4}/s$ was applied to these samples. All specimens have dimensions of $20 \times 10 \times 4$ mm³, Figure 7a.

The measured true stress-strain responses under off-axis compressive loading are compared with those predicted by the finite element model in Figure 8. In broad terms, the predictions capture the modulus, yield strength and hardening behaviour in the experiment for all the off-axis tests.

Two localised shear bands were observed in the 15° off-axis compression tests. Composite fibres in the UD composite typically undergo kinking in a narrow band under axial compression. Fibre kinking is plastic micro-buckling [46], which is facilitated by the rotation and buckling of misaligned fibres. The predicted shear band

compares to the measured contours under quasi-static loading in Figure 8a shows the accurate prediction of the fibre kinking effect. The numerical model is shown to be able to capture the plastic micro-buckling with a correct representation of plastic shear deformation and fibre rotation. We have also investigated the mesh size effect in capturing those localised deformation [44]. The maximum shear band width predicted from FE decreases with the decreasing mesh size, which is dependent on the geometric length scale such as fibre diameter [46]. Observations show typical values of band width in the neighbourhood of 10 fibre diameters. Therefore, a suitable choice of mesh size that is close to the geometric length scale will enable an accurate prediction of the localised deformation.

FE simulation accurately predicts the development of a shear band in the 45° off-axis experimental tests, as shown in Figure 8b. This is a failure mode essentially identical to that which would occur in the bulk matrix material, where fibres offer little resistance to applied loading. For a transverse compression test in the 90° off-axis, the two localised strain bands in the FE prediction, indicative of transverse slips, are similar to the observed strain contour, Figure 8c.

4.4 Shear tests of $[\pm 90^\circ]_{4s}$ composite laminates

Now we proceed to validate our model via comparison with the measured [2] stress-strain responses of $[\pm 90^\circ]_{4s}$ composite laminates made from AS4/PEKK carbon fibre thermoplastic composites. The material properties for AS4/PEKK can be found in Table 2 [2]. Virtual shear tests on $[\pm 90^\circ]_{4s}$ laminates were conducted under quasi-static ($\dot{\epsilon}_{QS} = 5 \times 10^{-4}/s$) conditions. The dimensions of the samples are specified in Figure 7b. Eight-node brick elements (C3D8R in the ABAQUS notation) with element size of 0.5 mm were used in the finite element model.

The proposed model is a lamina-level constitutive model, which is a general model for different layups. To model cross-ply composite laminates, we defined perfect-bonding between the neighbouring plies. This ensures strain compatibility under which a continuous and unique displacement field can be obtained. The deformation of an individual ply will be affected by the neighbouring plies due to the constraint of strain compatibility. Therefore, the cross-ply coupling effect is taken into account automatically.

Figure 9a shows the comparison between the experimental and numerical true shear stress-strain responses of $[\pm 90^\circ]_{4s}$ laminates under shear loading. Significant fibre rotation was present in the experimental tensile tests of $[\pm 90^\circ]_{4s}$ laminates and contributed to the non-linear hardening behaviour. The predictions are in very good agreement with the measured responses. In particular, the model is able to account for the fibre rotation and reproduces initial yield and linear hardening region for the shear test accurately. The mismatch of the stress-stress curves in the final regime of Figure 9a, results from the absence of a composite damage model in the crystal model. In the experiment, this is the regime where fibre breakage, matrix cracking and delamination are triggered [4]. Continuum damage models such as the combined plastic and smeared crack model [12] or the continuum shear damage model [2] have successfully captured the damage initiation and evolution in composite laminates. Since the focus of this study is the non-linear shear behaviour, incorporating continuum damage model with the crystal plasticity model is beyond the scope of the present study and will be addressed in forthcoming studies.

The predicted shear strain contours and fibre rotation of $[\pm 90^\circ]_{4s}$ composite laminates are compared to the measurements in Figure 9b. A good correlation between measured and numerically predicted shear strain contours were achieved. The

measured fibre rotation and predicted rotation are shown in Figure 9c and Figure 9d. The prediction provides accurate evaluation of the fibre rotation around $\varphi = 12^\circ \pm 2^\circ$, which is very close to the measured rotation angle.

The model is also capable to capture various loading conditions either under uniaxial loading or combined loading. We have demonstrated the model capability subjected to compressive loading in Figure 6c. We have also shown this model can predict mechanical behaviour under tensile loading and combined loading in another paper [44].

5. Concluding remarks

A phenomenological model was developed to predict the non-linear hardening behaviour of composite laminates under finite deformation. The large plastic matrix shearing and associated fibre rotations were captured through a framework based on a crystal plasticity model. Analytical models suggest the geometrical hardening behaviour of composite lamina is dependent on the longitudinal modulus and shear strain, whilst the transverse compressive response of composite lamina is governed by the matrix shear yield strength and slip directions. Finite element simulations of uniaxial compression on UD composite and shear tests of $[\pm 90^\circ]_{4s}$ composite laminates were conducted to validate this phenomenological model. Good qualitative and quantitative correlation was achieved between the numerical models and experimental results. The fidelity of the computational models was also able to provide detailed information on the plastic shear strain and fibre rotation.

Future work will focus on incorporating continuum damage mechanics to capture the evolution of matrix cracking and fibre breakage in the development of pseudo-ductile

[47], crashworthy [1,48] carbon fibre composites including a large amount non-linear shear failure.

Acknowledgement

The first author would like to gratefully acknowledge the start-up funding from Queen Mary University London. The authors thanks B.G. Liu for some useful discussions on this work.

References

- [1] W. Tan, B.G. Falzon, Modelling the crush behaviour of thermoplastic composites, *Compos. Sci. Technol.* 134 (2016) 57–71. doi:10.1016/j.compscitech.2016.07.015.
- [2] W. Tan, B.G. Falzon, Modelling the nonlinear behaviour and fracture process of AS4/PEKK thermoplastic composite under shear loading, *Compos. Sci. Technol.* 126 (2016) 60–77. doi:10.1016/j.compscitech.2016.02.008.
- [3] H. Koerber, J. Xavier, P.P. Camanho, High strain rate characterisation of unidirectional carbon-epoxy IM7-8552 in transverse compression and in-plane shear using digital image correlation, *Mech. Mater.* 42 (2010) 1004–1019. doi:10.1016/j.mechmat.2010.09.003.
- [4] H. Cui, D. Thomson, A. Pellegrino, J. Wiegand, N. Petrinic, Effect of strain rate and fibre rotation on the in-plane shear response of $\pm 45^\circ$ laminates in tension and compression tests, *Compos. Sci. Technol.* 135 (2016) 106–115. doi:10.1016/j.compscitech.2016.09.016.
- [5] F. Sket, A. Enfedaque, C. Alton, C. González, J.M. Molina-Aldareguia, J. Llorca, Automatic quantification of matrix cracking and fiber rotation by X-ray computed tomography in shear-deformed carbon fiber-reinforced laminates, *Compos. Sci. Technol.* 90 (2014) 129–138. doi:10.1016/j.compscitech.2013.10.022.
- [6] M. R. Wisnom, The effect of fibre rotation in ± 45 tension tests on measured shear properties, *Composites.* 26 (1995) 25–32. doi:10.1016/0010-4361(94)P3626-C.
- [7] E. Totry, J.M. Molina-Aldareguía, C. González, J. Llorca, Effect of fiber, matrix and interface properties on the in-plane shear deformation of carbon-fiber reinforced composites, *Compos. Sci. Technol.* 70 (2010) 970–980. doi:10.1016/j.compscitech.2010.02.014.
- [8] Z. Hashin, On elastic behaviour of fibre reinforced materials of arbitrary transverse phase geometry, *J. Mech. Phys. Solids.* 13 (1965) 119–134.

doi:10.1016/0022-5096(65)90015-3.

- [9] A. Puck, H. Schürmann, Failure analysis of FRP laminates by means of physically based phenomenological models, *Compos. Sci. Technol.* 62 (2002) 1633–1662. doi:10.1016/S0266-3538(01)00208-1.
- [10] S.T. Pinho, L. Iannucci, P. Robinson, Physically-based failure models and criteria for laminated fibre-reinforced composites with emphasis on fibre kinking: Part I: Development, *Compos. Part A Appl. Sci. Manuf.* 37 (2006) 63–73. doi:10.1016/J.COMPOSITESA.2005.04.016.
- [11] W. Tan, B.G. Falzon, L.N.S. Chiu, M. Price, Predicting low velocity impact damage and Compression-After-Impact (CAI) behaviour of composite laminates, *Compos. Part A Appl. Sci. Manuf.* 71 (2015) 212–226. doi:10.1016/j.compositesa.2015.01.025.
- [12] P.P. Camanho, M.A. Bessa, G. Catalanotti, M. Vogler, R. Rolfes, Modeling the inelastic deformation and fracture of polymer composites – Part II: Smearred crack model, *Mech. Mater.* 59 (2013) 36–49. doi:10.1016/J.MECHMAT.2012.12.001.
- [13] G. Catalanotti, P.P. Camanho, A.T. Marques, Three-dimensional failure criteria for fiber-reinforced laminates, *Compos. Struct.* 95 (2013) 63–79. doi:10.1016/J.COMPSTRUCT.2012.07.016.
- [14] L. Jia, L. Yu, K. Zhang, M. Li, Y. Jia, B.R.K. Blackman, J.P. Dear, Combined modelling and experimental studies of failure in thick laminates under out-of-plane shear, *Compos. Part B Eng.* (2016). doi:10.1016/j.compositesb.2016.08.017.
- [15] A. Sabik, Direct shear stress vs strain relation for fiber reinforced composites, *Compos. Part B Eng.* (2018). doi:10.1016/j.compositesb.2017.11.057.
- [16] C.T. Sun, C. Zhu, The effect of deformation-induced change of fiber orientation on the non-linear behavior of polymeric composite laminates, *Compos. Sci. Technol.* 60 (2000) 2337–2345. doi:10.1016/S0266-3538(00)00029-4.
- [17] B.R. Mauget, L. Minnetyan, C.C. Chamis, Large deformation nonlinear response of soft composite structures via laminate analogy, *J. Adv. Mater.* 34 (2001) 21–26.
- [18] U. Mandel, R. Taubert, R. Hinterhölzl, Three-dimensional nonlinear constitutive model for composites, *Compos. Struct.* 142 (2016) 78–86. doi:10.1016/J.COMPSTRUCT.2016.01.080.
- [19] T. Laux, K.W. Gan, J.M. Dulieu-Barton, O.T. Thomsen, A simple nonlinear constitutive model based on non-associative plasticity for UD composites: Development and calibration using a Modified Arcan Fixture, *Int. J. Solids Struct.* 162 (2019) 135–147. doi:10.1016/J.IJSOLSTR.2018.12.004.
- [20] M. Vogler, R. Rolfes, P.P. Camanho, Modeling the inelastic deformation and fracture of polymer composites – Part I: Plasticity model, *Mech. Mater.* 59 (2013) 50–64. doi:10.1016/J.MECHMAT.2012.12.002.
- [21] H. Koerber, P.P. Camanho, High strain rate characterisation of unidirectional

- carbon-epoxy IM7-8552 in longitudinal compression, *Compos. Part A*. 42 (2011) 462–470. doi:10.1016/j.compositesa.2011.01.002.
- [22] Y.F. Dafalias, The plastic spin concept and a simple illustration of its role in finite plastic transformations, *Mech. Mater.* 3 (1984) 223–233. doi:10.1016/0167-6636(84)90021-8.
- [23] R. Hill, A Theory of the Yielding and Plastic Flow of Anisotropic Metals, *Proc. R. Soc. A Math. Phys. Eng. Sci.* 193 (1948) 281–297. doi:10.1098/rspa.1948.0045.
- [24] N. Aravas, Finite-strain anisotropic plasticity and the plastic spin, *Model. Simul. Mater. Sci. Eng.* 2 (1994) 483–504. doi:10.1088/0965-0393/2/3A/005.
- [25] S. Eskandari, F.M. Andrade Pires, P.P. Camanho, A.T. Marques, Intralaminar damage in polymer composites in the presence of finite fiber rotation: Part I- Constitutive model, *Compos. Struct.* 151 (2016) 114–126. doi:10.1016/j.compstruct.2016.01.047.
- [26] R. Hill, J.R. Rice, Constitutive analysis of elastic-plastic crystals at arbitrary strain, *J. Mech. Phys. Solids.* 20 (1972) 401–413. doi:10.1016/0022-5096(72)90017-8.
- [27] R.J. Asaro, *Micromechanics of Crystals and Polycrystals*, *Adv. Appl. Mech.* 23 (1983) 1–115. doi:10.1016/S0065-2156(08)70242-4.
- [28] B.G. Liu, K. Kandan, H.N.G. Wadley, V.S. Deshpande, Deep penetration of ultra-high molecular weight polyethylene composites by a sharp-tipped punch, *J. Mech. Phys. Solids.* 123 (2019) 80–102. doi:10.1016/J.JMPS.2018.06.001.
- [29] B.G. Liu, K. Kandan, H.N.G. Wadley, V.S. Deshpande, High strain rate compressive response of ultra-high molecular weight polyethylene fibre composites, *Int. J. Plast.* (2019). doi:10.1016/j.ijplas.2019.04.005.
- [30] C. González, J. LLorca, Mechanical behavior of unidirectional fiber-reinforced polymers under transverse compression: Microscopic mechanisms and modeling, *Compos. Sci. Technol.* 67 (2007) 2795–2806. doi:10.1016/j.compscitech.2007.02.001.
- [31] W. Tan, F. Naya, L. Yang, T. Chang, B.G. Falzon, L. Zhan, J.M. Molina-Aldareguía, C. González, J. Llorca, The role of interfacial properties on the intralaminar and interlaminar damage behaviour of unidirectional composite laminates: Experimental characterization and multiscale modelling, *Compos. Part B Eng.* 138 (2017) 206–221. doi:10.1016/j.compositesb.2017.11.043.
- [32] R.J. Asaro, A. Needleman, Overview no. 42 Texture development and strain hardening in rate dependent polycrystals, *Acta Metall.* 33 (1985) 923–953. doi:10.1016/0001-6160(85)90188-9.
- [33] R.J. Asaro, Crystal Plasticity, *J. Appl. Mech.* 50 (1983) 921. doi:10.1115/1.3167205.
- [34] P.G. Partridge, The crystallography and deformation modes of hexagonal close-packed metals, *Metall. Rev.* 12 (1967) 169–194. doi:10.1179/mtlr.1967.12.1.169.

- [35] F. Barlat, D.J. Lege, J.C. Brem, A six-component yield function for anisotropic materials, *Int. J. Plast.* 7 (1991) 693–712. doi:10.1016/0749-6419(91)90052-Z.
- [36] A. Puck, H. Schürmann, Failure analysis of FRP laminates by means of physically based phenomenological models, *Compos. Sci. Technol.* 58 (1998) 1045–1067. doi:10.1016/S0266-3538(96)00140-6.
- [37] B. Paul, A modification of the coulomb-mohr theory of fracture, *J. Appl. Mech. Trans. ASME.* 28 (1960) 259–268. doi:10.1115/1.3641665.
- [38] C.G. Davila, P.P. Camanho, C.A. Rose, Failure Criteria for FRP Laminates, *J. Compos. Mater.* 39 (2005) 323–345. doi:10.1177/0021998305046452.
- [39] F. Naya, C. González, C.S. Lopes, S. Van Der Veen, F. Pons, Computational micromechanics of the transverse and shear behavior of unidirectional fiber reinforced polymers including environmental effects, (2017). doi:10.1016/j.compositesa.2016.06.018.
- [40] T. Chang, L. Zhan, W. Tan, Void content and interfacial properties of composite laminates under different autoclave cure pressure, *Compos. Interfaces.* 24 (2017) 529–540. doi:10.1080/09276440.2016.1237113.
- [41] E. Schmid, W. Boas, *Kristallplastizität mit besonderer Berücksichtigung der Metalle*, 1935. doi:10.1017/CBO9781107415324.004.
- [42] W. a. Spitzig, O. Richmond, Effect of Hydrostatic Pressure on the Deformation Behavior of Polyethylene and Polycarbonate in Tension and in Compression, *Polym. Eng. Sci.* 19 (1979) 1129–1139. doi:10.1002/pen.760191602.
- [43] K.D. Pae, K.Y. Rhee, Effects of hydrostatic pressure on the compressive behavior of thick laminated 45 ° and 90 ° unidirectional graphite-fiber/epoxy-matrix composites, *Compos. Sci. Technol.* 53 (1995) 281–287. doi:10.1016/0266-3538(94)00080-8.
- [44] W. Tan, B. Liu, A physically-based constitutive model for the shear-dominated response and strain rate effect of carbon fibre reinforced composites, *Compos. Part B Eng.* 193 (2020) 108032. doi:10.1016/j.compositesb.2020.108032.
- [45] J.D. Schaefer, B.T. Werner, I.M. Daniel, Strain-Rate-Dependent Failure of a Toughened Matrix Composite, *Exp. Mech.* 54 (2014) 1111–1120. doi:10.1007/s11340-014-9876-0.
- [46] B. Budiansky, N.A. Fleck, Compressive failure of fibre composites, *J. Mech. Phys. Solids.* 41 (1993) 183–211. doi:10.1016/0022-5096(93)90068-Q.
- [47] J.D. Fuller, M.R. Wisnom, Pseudo-ductility and damage suppression in thin ply CFRP angle-ply laminates, *Compos. Part A Appl. Sci. Manuf.* 69 (2015) 64–71. doi:10.1016/J.COMPOSITESA.2014.11.004.
- [48] B.G. Falzon, W. Tan, Virtual Testing of Composite Structures: Progress and Challenges in Predicting Damage, Residual Strength and Crashworthiness, in: *Struct. Integr. Carbon Fiber Compos.*, 2016.
- [49] C. González, J. Llorca, Multiscale modeling of fracture in fiber-reinforced composites, (2006). doi:10.1016/j.actamat.2006.05.007.

- [50] H. Koerber, P. Kuhn, M. Ploeckl, F. Otero, P.-W. Gerbaud, R. Rolfes, P.P. Camanho, Experimental characterization and constitutive modeling of the non-linear stress-strain behavior of unidirectional carbon-epoxy under high strain rate loading, *Adv. Model. Simul. Eng. Sci.* 5 (2018) 17. doi:10.1186/s40323-018-0111-x.

Figures

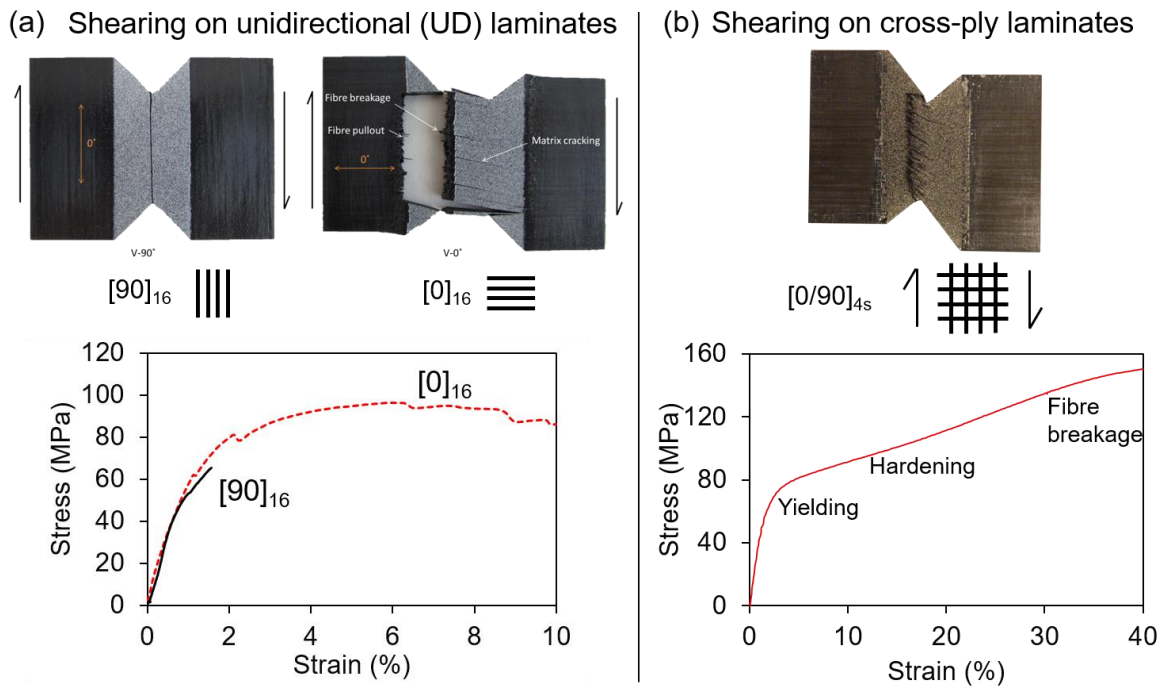


Figure 1. The failure modes and stress-strain curves of V-notched shear tests of AS4/PEKK carbon fibre thermoplastic composites [2]. (a) Shear loading is applied parallel and perpendicular to fibre direction on the unidirectional laminates (b) shear loading is applied on cross-ply laminates.

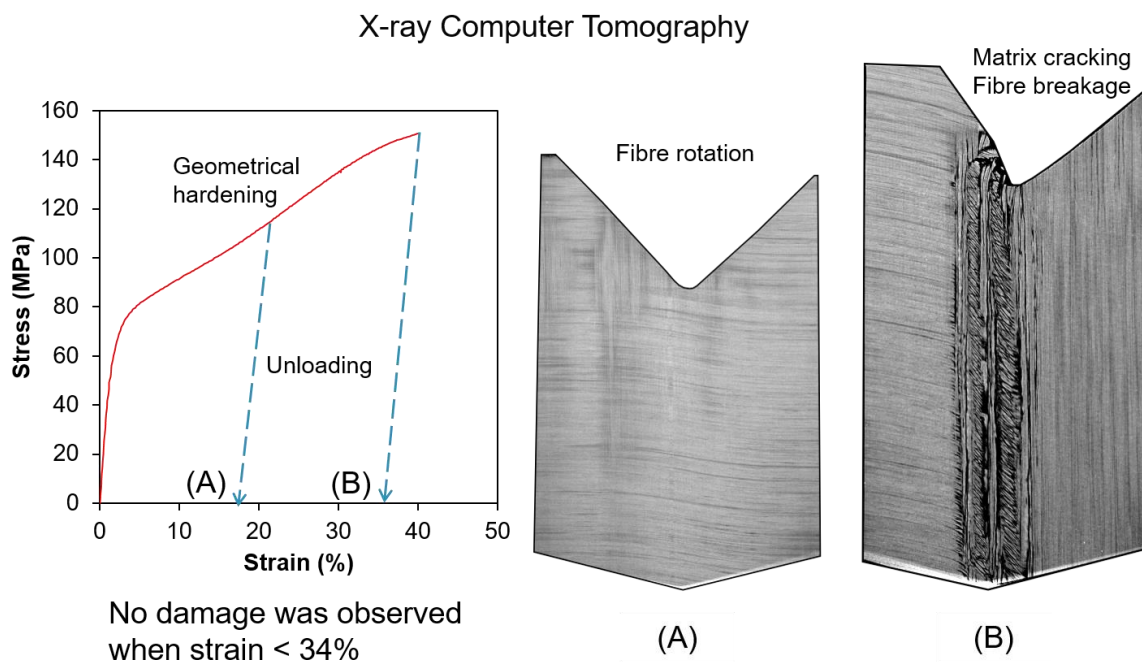


Figure 2. X-ray Computer Tomography (CT) scans reveal the fibre rotation and matrix deformation or cracking at the strain of 18% and 35% after unloading.

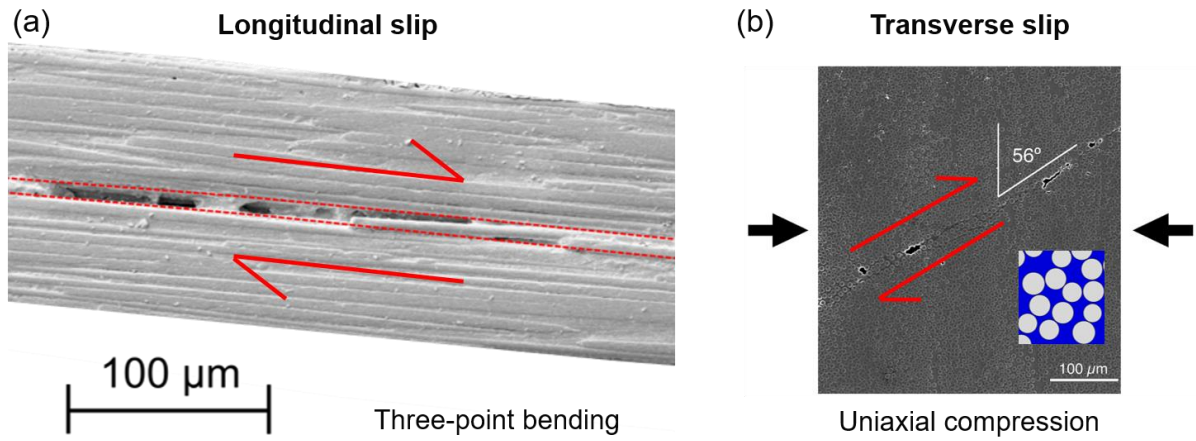


Figure 3. (a) Longitudinal slip observed in the short beam three-point bending test of CFRP [31] (b) Transverse slip when uniaxial compression loading is applied on the CFRP [49].

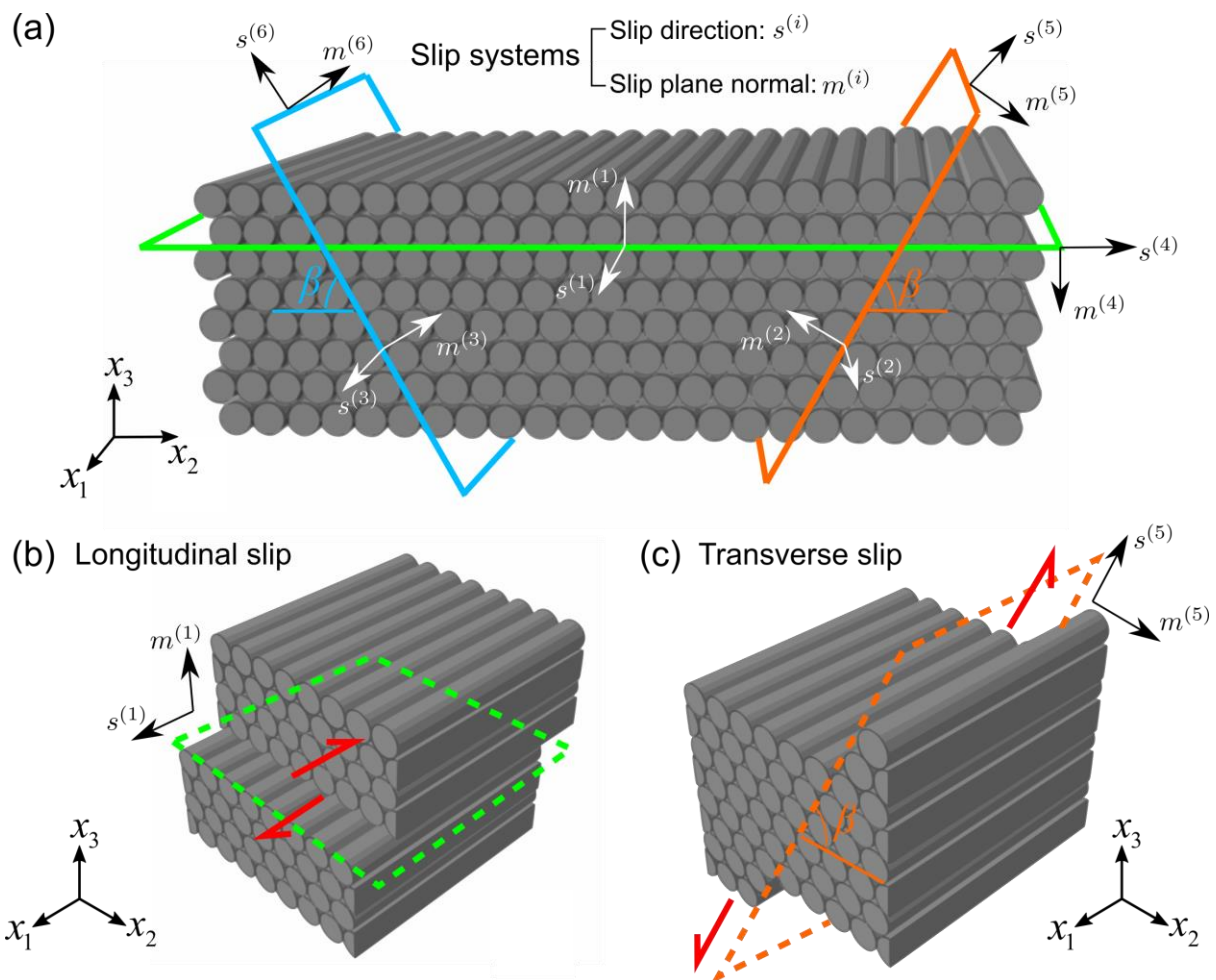


Figure 4. Sketches of (a) six typical slip systems with slip direction $s^{(\alpha)}$ and slip plane normal $m^{(\alpha)}$. (b) The slip system $(s^{(1)}, m^{(1)})$ in the longitudinal direction and (c) the slip system $(s^{(5)}, m^{(5)})$ in the transverse direction.

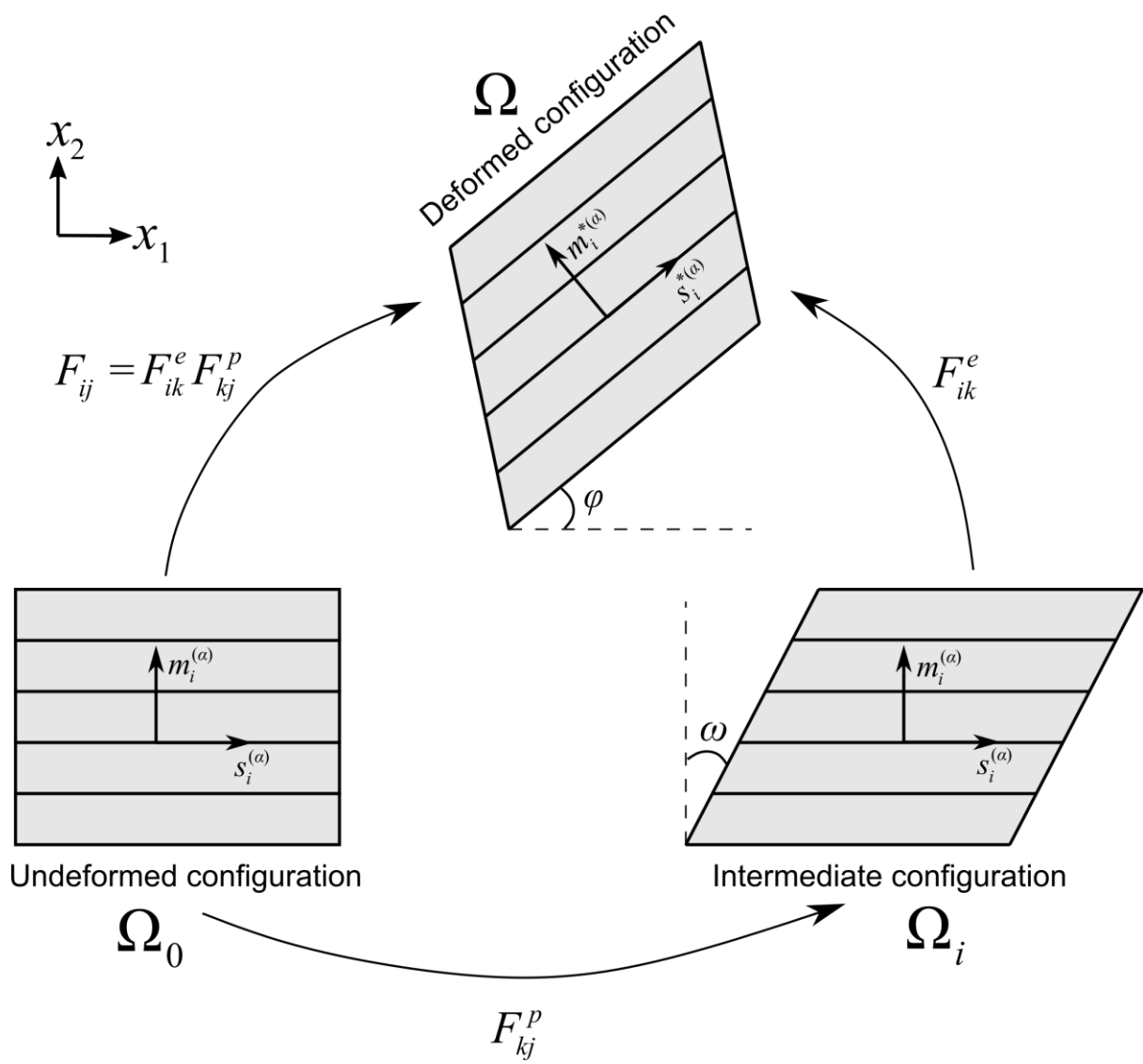


Figure 5. Multiplicative decomposition of the total deformation gradient into elastic and plastic component.

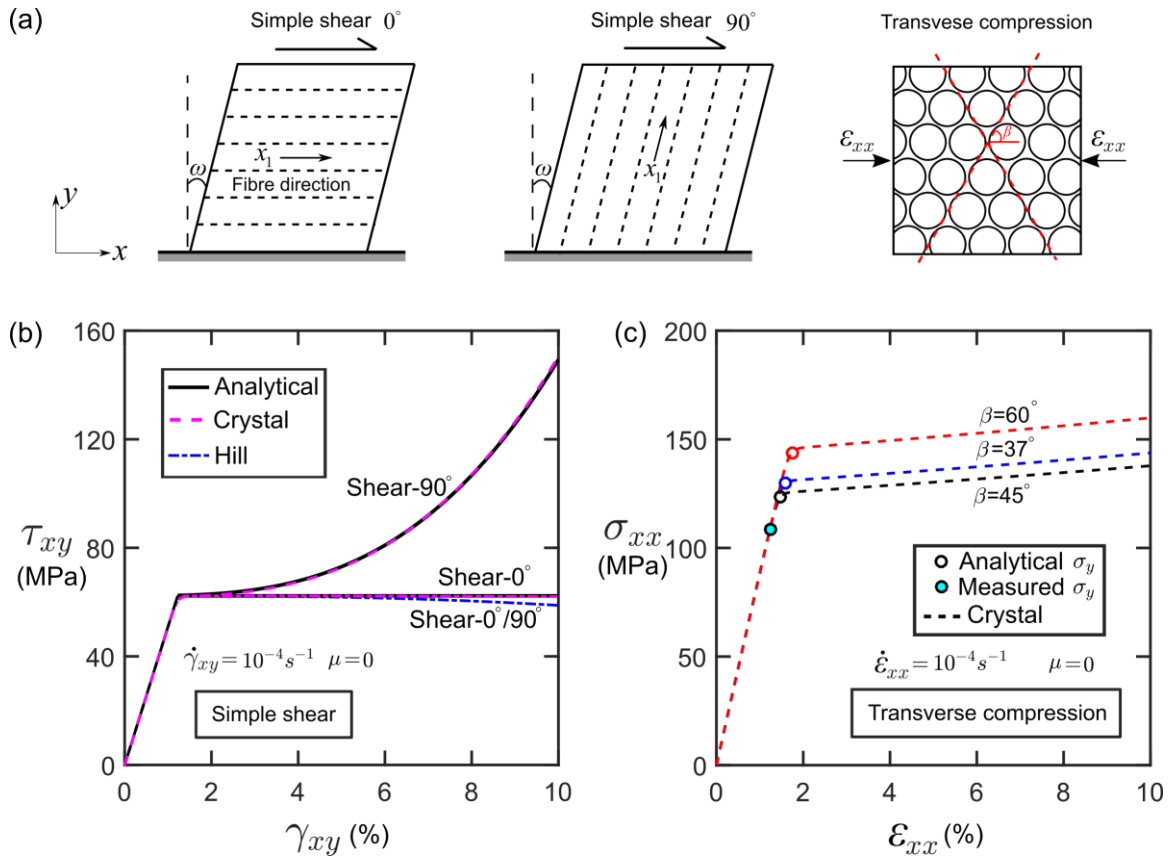


Figure 6. (a) Sketches of boundary conditions: simple shear 0° , simple shear 90° , transverse compressive tests of a unidirectional lamina. (b) Predicted stress-strain curves of simple shear on a unidirectional lamina using the crystal plasticity model and Hill's model. (c) Predicted stress-strain curves of a unidirectional lamina under transverse compression of slip system oriented at $\beta = 37^\circ, 45^\circ, 60^\circ$ respectively.

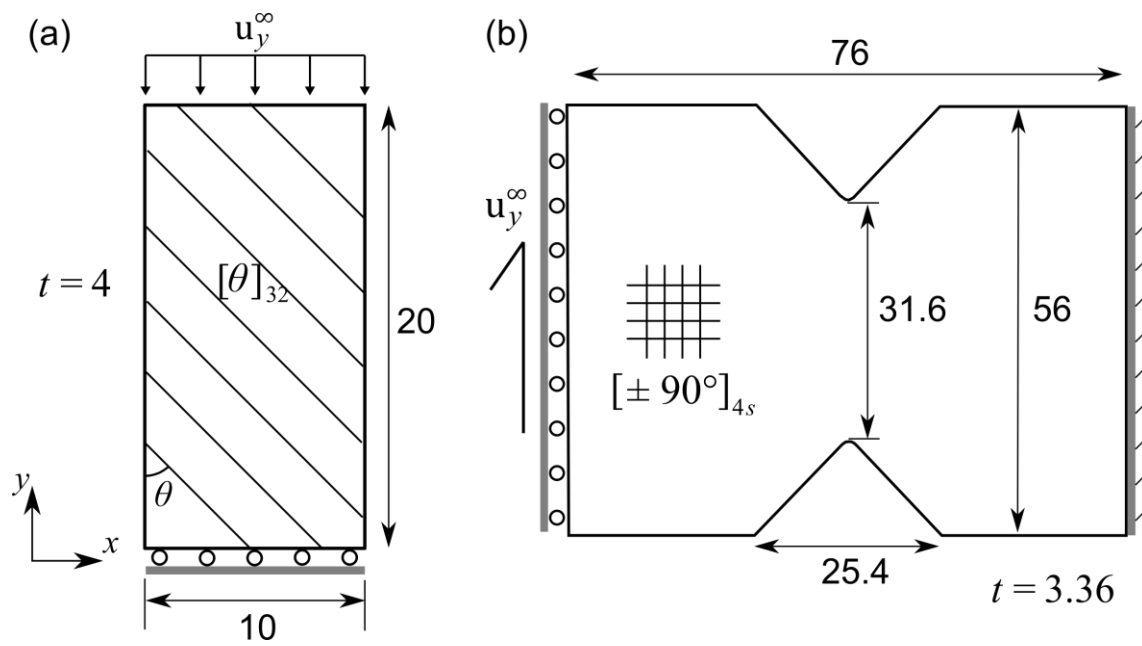


Figure 7. Specimen geometries for (a) IM7-8552 unidirectional composite laminates of different off-axis angle subject to uniaxial compressive loading [3] and (b) AS4-PEKK cross-ply composite laminates subject to shear loading. Note that thickness is denoted by t . All units are in mm.

Uniaxial compression under quasi-static loading

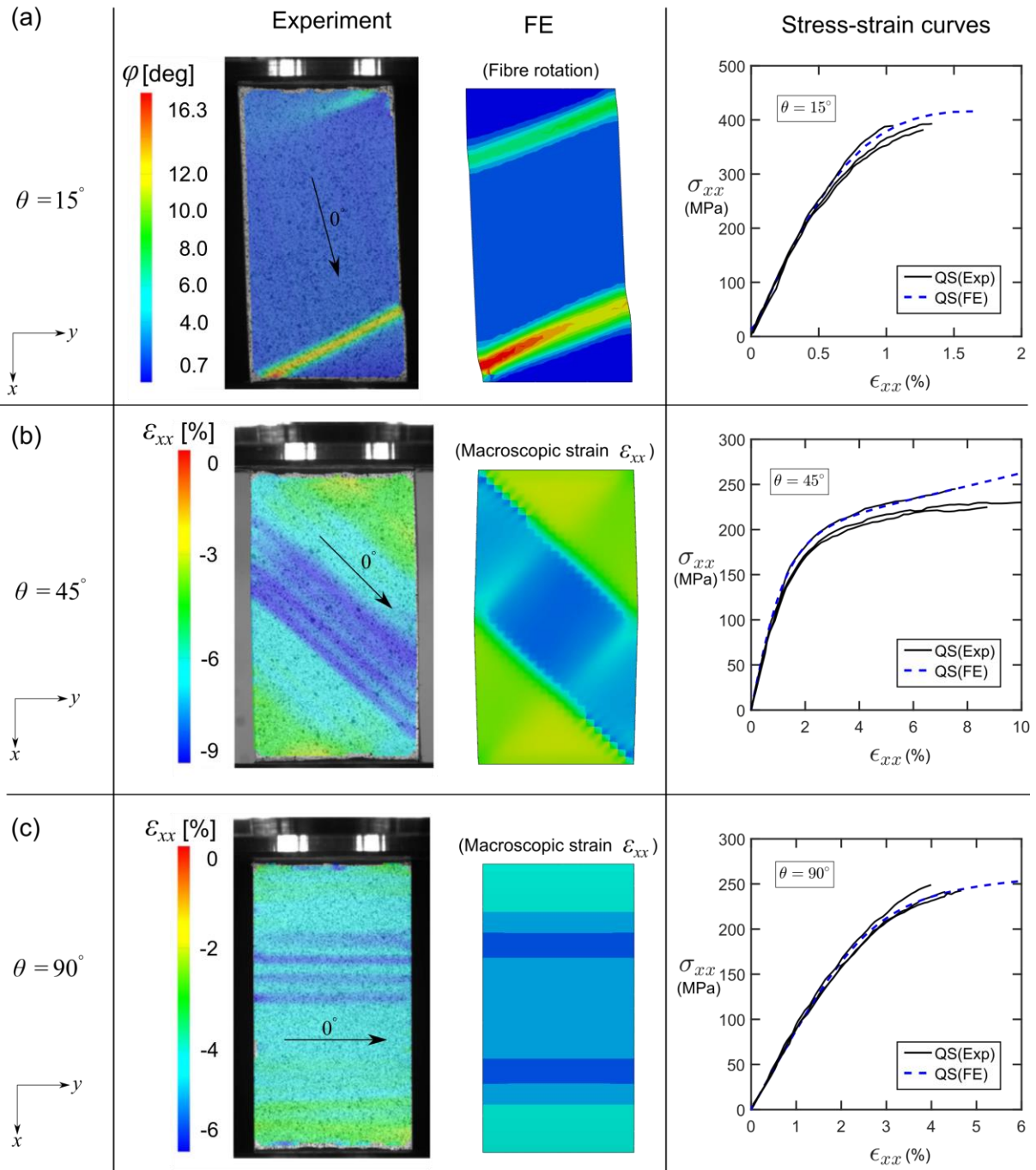


Figure 8. Measured [3] and predicted fibre rotation, axial compressive strain and stress-strain curves for off-axis (a) $\theta = 15^\circ$ (b) $\theta = 45^\circ$ and (c) $\theta = 90^\circ$ compression tests subjected to quasi-static loading.

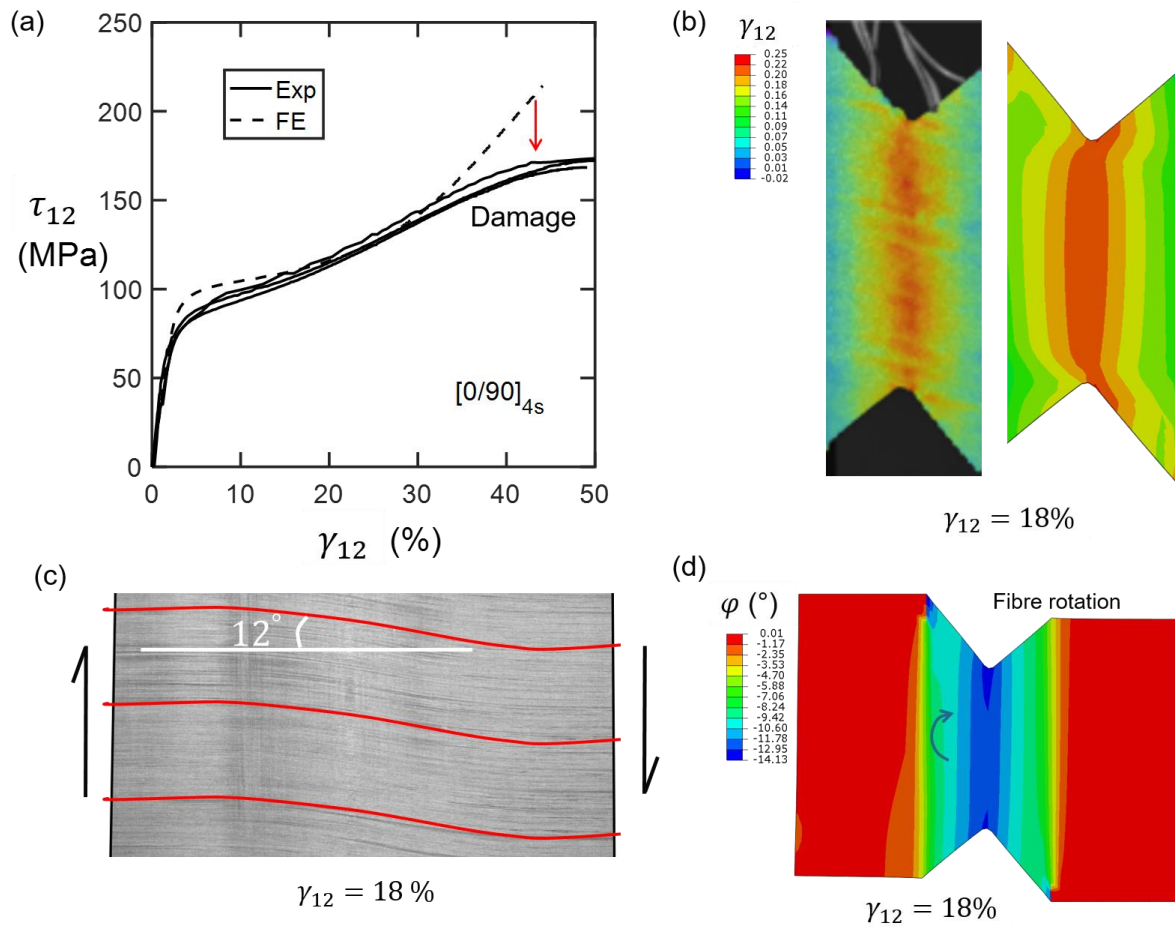


Figure 9. (a) Measured [2] and predicted shear stress-strain responses. (b) Measured and predicted shear strain contour. (c) The measured and predicted (d) fibre rotation.

Tables

Table 1. Slip direction vectors and slip plane normal vectors

Slip systems α	Slip direction $s^{(\alpha)}$	Slip plane normal $m^{(\alpha)}$
Longitudinal slip systems	(1) (1, 0, 0)	(0, 1, 0)
	(2) (1, 0, 0)	(0, $-\sin \beta$, $\cos \beta$)
	(3) (1, 0, 0)	(0, $\sin \beta$, $\cos \beta$)
Transverse slip systems	(4) (0, 1, 0)	(0, 0, -1)
	(5) (0, $\cos \beta$, $\sin \beta$)	(0, $\sin \beta$, $-\cos \beta$)
	(6) (0, $-\cos \beta$, $\sin \beta$)	(0, $\sin \beta$, $\cos \beta$)

Table 2. Material parameters for finite element simulation of IM7-8552 and AS4-PEKK carbon fibre composites [2,3,50]

Material properties	IM7-8552	AS4-PEKK
E_f	171.42 GPa	138 GPa
ν_{12}	0.32	0.3
ν_{23}	0.34	0.3
E_m	8.93 GPa	10.3 GPa
G_{12}	5.10 GPa	5.2 GPa
μ	0.28	0.28
τ_y	62.3 MPa	80.81 MPa
σ_{my}	104 MPa	254 MPa
n	22.4	22.4